Supporting information

Unlock Flow-type Reversible Aqueous Zn-CO_2 Batteries

Muhammad Kashif Aslam, Herui Wang, Zhihao Nie, Sheng Chen, Qiang Li* and Jingjing Duan*

School of Energy and Power Engineering, MIIT Key Laboratory of Thermal Control of Electronic Equipment, School of Chemistry and Chemical Engineering, Nanjing University of Science and Technology, Nanjing 210094, P. R. China

E-mail: liqiang@mail.njust.edu.cn; jingjing.duan@njust.edu.cn

Table of Contents

Experimental section

Figure S11. Comparison of eCO_2RR Faradaic Efficiencies (FEs) for all three prepared catalytic materials: FEs for Formate ($HCOO^-$) (a), FEs for hydrogen (H2) (b), and FEs for carbon monoxide (CO) (c).

Figure S12. FE's of different products based on H-cell eCO_2RR.

Figure S13. Double layer capacitance investigation of Pd/SnO_2@C. Cyclic voltammetry curves at different scan rates (a). Overall response of current density against different scan rates (b).

Figure S14. Double layer capacitance investigation of SnO_2@C. Cyclic voltammetry curves at different scan rates (a). Overall response of current density against different scan rates (b).

Figure S15. Double layer capacitance investigation of Pd@C. Cyclic voltammetry curves at different scan rates (a). Overall response of current density against different scan rates (b).

Figure S16. Models structures of Pd@C (a), SnO_2@C (b) and Pd/SnO_2@C (c).

Figure S17. OCP curves presenting response against CO_2 and Ar supply for Pd@C (a) and SnO_2@C (b) based on flow type cell.

Figure S18. Polarization charge-discharge curves for both H-cell flow type cell based Zn-CO_2 batteries (a) and corresponding power densities curves (b).

Figure S19. Comparison of power densities with previously reported works.

Figure S20. Overall charge-discharge response at different current rate based on homemade flow type cell.

Figure S21. Digital photograph of a single bulb illuminated by a 3-series of aqueous Zn-CO_2 batteries (a) and a digital clock power by single Zn-CO_2 battery (b).

Figure S22. pH values measured at different pre-saturating CO_2 time.

Table S1. Energy efficiencies (EE) of the aqueous rechargeable reversible Zn-CO_2 battery at different applied current densities.

Table S2. Comparison of aqueous Zn-CO_2 battery performance with previously reported works.

Experimental section

Synthesis of Sn-MOF

All procured chemicals were of analytical grade and used as received. To synthesize Sn-MOF, 2.4mM sodium hydroxide and 1.2mM phthalic acid were dissolved in a 60mL solution of DMF (Dimethylformamide) and DI (Deionized) water at a volume ratio of 1:1 to form mixture A. Concurrently, a 0.015 M solution of tin sulfate was prepared by dissolving it in 10 mL of DI water to form mixture B. Subsequently, mixture B was rapidly added to mixture A under rigorous stirring, which continued at 50 °C for 2 hours. After this period, the resulting white precipitates were washed thrice with DMF before being transferred to DI water. Once the precipitates settled, the water was replaced three times. Finally, the precipitates were dried under vacuum conditions at 60 °C.

Synthesis of SnO_2@C, Pd/SnO_2@C and Pd@C

For the synthesis of Pd/SnO_2@C, Sn-MOF was initially calcined at 400°C under an atmosphere of 10% H_2/Ar for 4 hours at a heating rate of 5°C per minute. This process yielded SnO_2@C. Following this, 100 mg of SnO_2@C and 70 mg of Pd source were dispersed in ethylene glycol (EG). Then, a 1M NaOH solution was added to maintain a pH of 13 to enhance the precipitation. The mixture was sealed in Teflon and heated at 140°C for 1 hour. After cooling to room temperature, a 0.1M HNO_3 solution was gradually added to reduce the pH to 3. The product was then washed with water until it reached neutral pH. Finally, the prepared material was calcined at 300°C for 2 hours under a H_2/Ar atmosphere. For the preparation of Pd@C, the same procedure was followed, with carbon being used instead of SnO_2@C.

eCO_2RR measurements

All CO_2 electrocatalytic reduction measurements were carried out in both a three-chamber flow cell and a typical H-type cell. The $KHCO_3$ (0.5 M) electrolyte was pumped continuously into the cathodic and anodic chambers at a flow rate of 5 mL per minute. An Anion Exchange Membrane (AEM) separating the anodic and cathodic chambers prevented the reduced liquid products from mixing with the anolyte. Additionally, CO_2 was purged into the third chamber, known as the gas chamber, and beside the Gas Diffusion Electrode (GDE) layer at a flow rate of 80 sccm. All electrochemical experiments were conducted using a CHI760e workstation. A titanium plate coated with iridium and a KCl-saturated Ag/AgCl electrode served as the counter electrode and reference electrode, respectively. The working electrode was prepared from the catalyst mixed with isopropyl alcohol and DI water (3:1 ratio), along with Nafion solution, and supported on gas diffusion carbon paper. Linear Sweep Voltammetry (LSV) curves were recorded over a potential range from 0 to -3V at a scan rate of 5 mV per second. The Electrochemical Surface Area (ECSA) was determined between 0.2 and 0.3V. Electrochemical Impedance Spectroscopy (EIS) was performed in the range of $0.01\text{-}10^6$ Hz with an applied potential of -0.2 V *vs*. RHE. All potentials in all electrochemical experiments were converted to the Reversible Hydrogen Electrode (RHE) reference scale using the following equation:

$$E_{RHE} = E_{Ag/AgCl} + 0.0591 \times pH + 0.197\ V$$

Computational methods and Models

First-principles calculations are performed using the MedeA-VASP based on DFT within the plane wave basis set approach.[1, 2] The electron-ion interactions are described by the Density function method,[3] and the electron-electron exchange correlations are described by the Perdew-Burke-Ernzerhof (PBE) functional.[4]

For the structure optimization, we use the RMM-DIIS update algorithm. We use low precision for efficient computation and normal precision for accurate computation. The convergence is 0.06 and 0.05 for efficiency and accuracy computation. Both efficiency and accuracy computation use 400 eV planewave cutoff. A Gaussian smearing with a width of 0.05 eV was also utilized. For the surface Brillouin zone integration, a 1 × 1 × 1 Monkhorst−Pack kpoint mesh was used. The convergence criteria for electronic self-consistent iteration and ionic relaxation were set to 10^{-4} eV and 10^{-5} eV. Hubbard-U correction method (DFT+U) was carried out to improve the description of highly correlated Bi 3d orbital with the value of U set to standard LDA or GGA.

The charge difference was computed through the following equation:

$$\rho_{diff} = \rho_{abs} - \rho_{atom}$$

where ρ_{abs} is the electron distribution of the overall system, ρ_{atom} is from corresponding atom systems.

The detailed Gibbs free energy calculation for eCO_2RR has been carried out as it follows: ($G = E + Gcorr$). In Gcorr, the zero-point energies and entropic contributions were included ($Gcorr = ZPE – TS$).[5]

Zn-CO_2 battery assembly

Anode preparation: First, zinc metal plate was polished with sand paper and then ultrasonically cleaned with acetone and ultrapure water (50% each), then cut it into the size of 3 x 3 cm and dry it for standby. The electrolyte of the anode was 6 M KOH+0.02 M of zinc acetate to get a certain concentration of Zn ions. Preparation of cathode: 10 mg of Pd/SnO_2@C catalyst was taken with isopropanol and DI water in the ratio of 3:1 and ultrasound for 1 hr. A spray gun was used to spray ~6 mg of the sample onto the hydrophobic carbon paper (3 x 3 cm) and dried on hot surface. The area of the sample coated on the carbon paper was 1 x 1 cm. The catholyte used in cathode chamber was CO_2-saturated 0.8 M $KHCO_3$. In fact, we utilized a $KHCO_3$ solution as a catholyte in eCO_2RR and achieved over 98% production of $HCOO^-$. This is why we employed same catholyte in the Zn-CO_2 battery, aiming to replicate the same electrolyte effect observed in eCO_2RR and the battery. 3) Battery assembly: The anode and cathode electrodes of Zn-CO_2 battery were separated with BPM membrane and both chambers were filled with anolyte and catholyte with an extra gas chamber on cathode side for gas flow. The charge-discharge polarization curves were collected at the scan rate of 5 mV s^{-1} under continues supply of CO_2 gas.

Characterizations

The structural morphology and composition of the catalyst were analyzed by scanning electron microscopy (SEM) and high-resolution transmission electron microscopy (HRTEM, JEM-2100F, 200 kV), respectively. X-ray diffraction (XRD, Bruker, D8 Advance A25, Co target, Kα 1=1.78897 Å, 0.02 mm thick Fe filter) was used to check purity and crystallinity of as prepared catalytic material. X-ray photoelectron spectroscopy (XPS, PHI 5000 VersaProbe) was also performed to confirm the oxidation states of the atoms.

Calculation for theoretical energy efficiency of aqueous Zn-CO_2 battery:

The theoretical energy efficiency can be calculated using the following equation:

$$\mathrm{EE} = \frac{\Delta G_{\text{output}}}{\Delta G_{\text{input}}} = \frac{nE_{\text{discharge}}F + \Delta G_{CO_2\ \text{spliting}}}{nE_{\text{charge}}F}$$

$$\Delta G_{CO_2\ \text{splitting}} = 257.38\mathrm{kJ\ mol^{-1}}$$

In the real cell, competitive HER produces fuel H_2, while carbon dioxide reduction also produces a small amount of CO, considering that, battery EE can be calculated as follows:

$$\mathrm{EE} = \frac{\Delta G_{\text{output}}}{\Delta G_{\text{input}}} = \frac{nE_{\text{discharge}}F + FE_{HCOO^-} \times \Delta G_{CO_2\ \text{spliting}} + FE_{CO} \times \Delta G_{CO_2\ \text{spliting}} + FE_{HER} \times \Delta G_{H_2O\ \text{spliting}}}{nE_{\text{charge}}F}$$

$$\Delta G_{H_2O\ \text{splitting}} = 257.38\mathrm{kJ\ mol^{-1}}$$

Calculation for theoretical energy density of aqueous Zn-CO_2 battery

The theoretical potential (V) calculation of aqueous reversible Zn-CO_2 cells:

To calculate theoretical potential, anodic and cathodic potentials needs to calculate according to the produced CO_2RR major product.

Cathodic potential: during discharge process of Zn-CO_2 battery following reaction will take place;

$CO_2 + 2H^+ + 2e^- \rightarrow HCOOH$ under 0.8 M $KHCO_3$, sat.CO_2 solution with pH=4.5 conditions:

$$E_c = E^{\theta}_{CO_2/HCOOH} - \frac{RT}{nF}\ln\left[\frac{1}{\alpha^2_{H^+}}\right] \Rightarrow 0.02V - \frac{8.314\times 298.15}{2\times 96485}\ln\left[\frac{1}{(10^{-4.5})^2}\right] V{=}{-0.246V}$$

Where $E^{\theta}_{CO_2/HCOOH} = 0.02V$ *vs.* SHE

Anodic potential: During charge process of Zn-CO_2 battery following reactions take place;

Under 6 M KOH + 0.02 M Zn(ac):

$$Zn \rightarrow Zn^{2+} + 2e^{-}$$

$$Zn^{2+} + 4OH^{-} \rightarrow Zn(OH)_4^{2-}$$

$$Zn(OH)_4^{2-} \rightarrow ZnO + 2OH^{-} + H_2O$$

$$E_a = E^{\theta}_{Zn(OH)_4^{2-}} - \frac{RT}{nF}\ln\left[\frac{1}{\alpha_{Zn(OH)_4^{2-}}}\right] \Rightarrow -1.199V - \frac{8.314\times298.15}{2\times96485}\ln\left[\frac{1}{0.02}\right] V\text{=-}1.249\ V$$

Where $E^{\theta}_{Zn(OH)_4^{2-}/Zn} = -1.199V\ vs.$ SHE

And overall battery reaction will be written as follow:

$$CO_2 + Zn + 2H^{+} + 2OH^{-} \rightarrow ZnO + HCOOH + H_2O$$

Note that: where, R is 80314 J K^{-1} mol^{-1}, F is Faradaic constant 96485 C mol^{-1}, T is 298.15 K, and n is number of electrons transfer during CRR.

So, the theoretical potential will be:

$$E_{theo} = E_c - E_a \Rightarrow -0.246 - (-1.249) = 1.0028V$$

And theoretical energy density of the Zn-CO$_2$ battery could be:

$$ED_{Zn-CO_2} = C_{Zn} \times E_{theo} \Rightarrow 825 \times 1.0028 = 827.3\ Wh\ kg^{-1}$$

Where, C_{zn} is the theoretical capacity of the Zn anode based battery, which is 825 mAh g^{-1}.

In the above calculation of theoretical potential 0.8M KHCO3 solution with 4.5 pH was considered. In fact, we designed a method for pre-saturating CO$_2$ before the aqueous Zn-CO$_2$ battery test: CO$_2$ gas was continuously injected into KHCO$_3$ solution with bubble dispersed gas for several hours. When CO$_2$ is dissolved into a solution of KHCO$_3$ (Potassium bicarbonate), a reaction occurs that forms K_2CO_3 (Potassium carbonate), H_2O (Water), and H_2CO_3 (Carbonic acid). The overall chemical reaction is:

$$2KHCO_3 + CO_2 \rightarrow K_2CO_3 + H_2O + H_2CO_3$$

$$H_2CO_3 \rightarrow HCO_3^- + H^+$$

H_2CO_3 is a weak acid and it can further dissociate into H^+ (Hydrogen ions) and HCO_3^- (Bicarbonate ions), which subsequently decreases the pH of the solution. A lower pH means a more acidic solution, so the introduction of CO_2 makes the solution more acidic due to the formation of carbonic acid and the measured pH was about 4.53 as shown in **Figure S22.**

In addition, During CO_2RR, carbon dioxide (CO_2) is reduced to form other product, commonly carbon-based products like methane (CH_4), ethylene (C_2H_4), or even formate ($HCOO^-$). The reduction of CO_2 typically involves the transfer of electrons and protons. These additional protons can come from water molecules (H_2O) in the electrolyte solution, which dissociate to produce H^+ ions and OH^-.

$CO_2 + e^- + H^+ \rightarrow \text{Product} + H^+$

When the concentration of H^+ ions increases compared to OH^-, the pH of the solution decreases because pH is inversely related to $[H^+]$. Therefore, as $[H^+]$ goes up, pH goes down, meaning the solution becomes more acidic.

In addition, if the product of CO_2RR is an acid, such as formic acid (HCOOH) for example, that will also contribute to a decrease in pH. Formic acid can dissociate in solution to form H^+ and formate anion ($HCOO^-$), increasing the concentration of H^+ in solution and thereby lowering the pH.

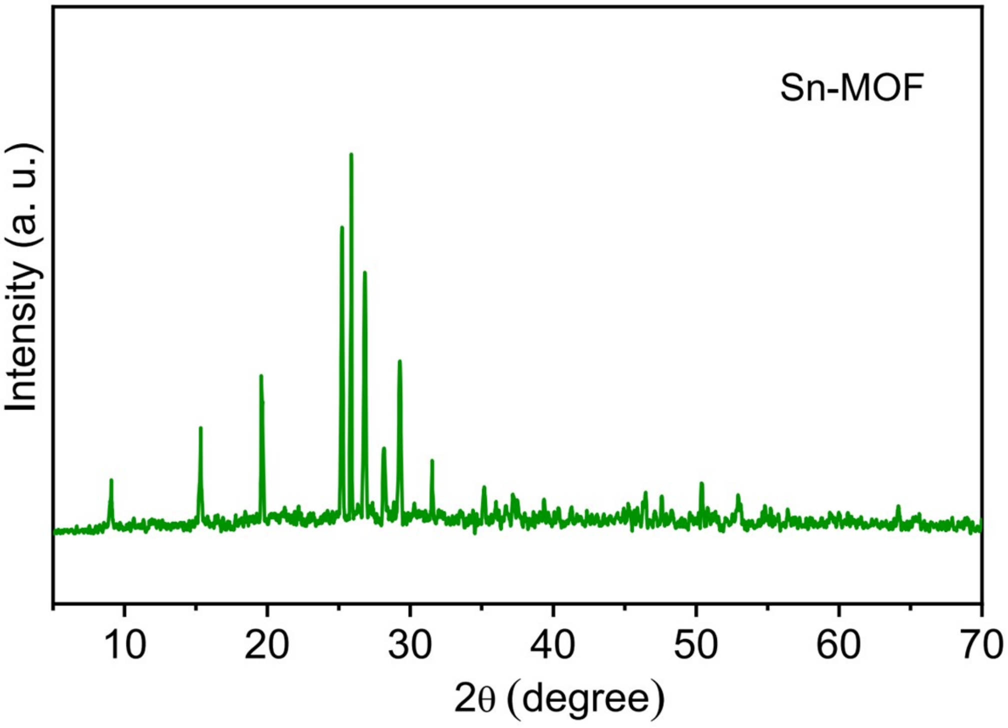

Fig. S1. XRD pattern of Sn-MOF.

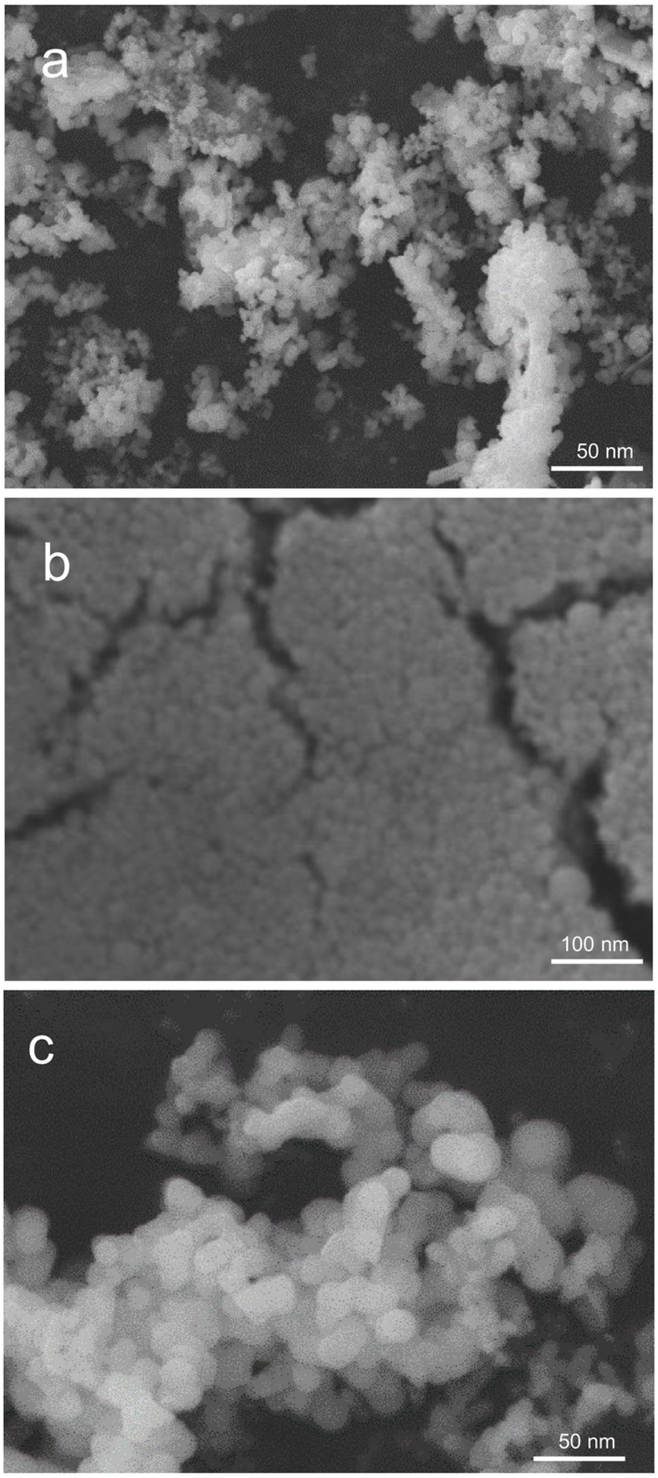

Fig. S2. SEM images of Sn-MOF (a), SnO_2@C (b) and Pd/SnO_2@C (c).

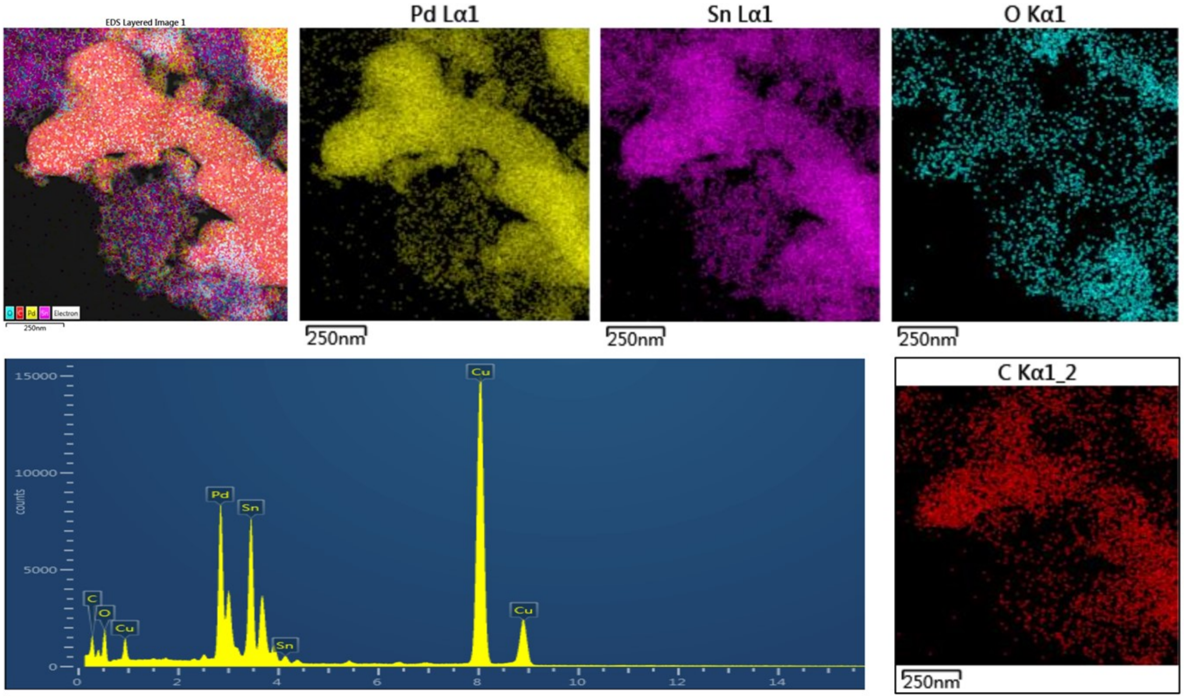

Fig. S3. EDS colour mapping and EDS spectrum of $Pd/SnO_2@C$.

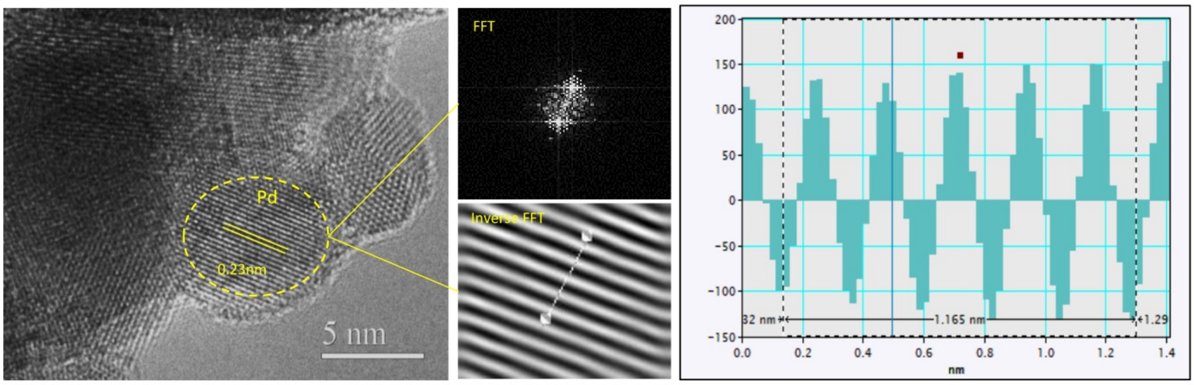

Fig. S4. HRTEM image of Pd/SnO_2@C presenting Pd site.

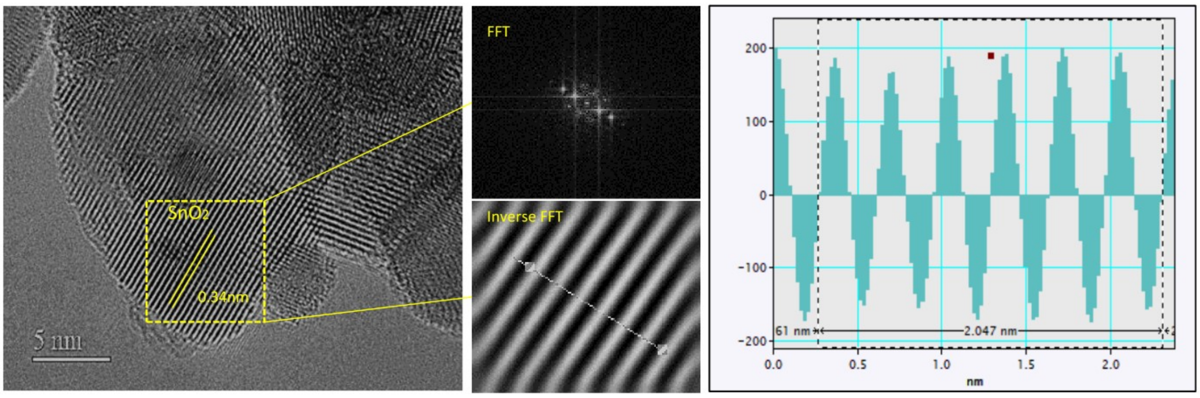

Fig. S5. HRTEM image of Pd/SnO_2@C presenting SnO_2 site.

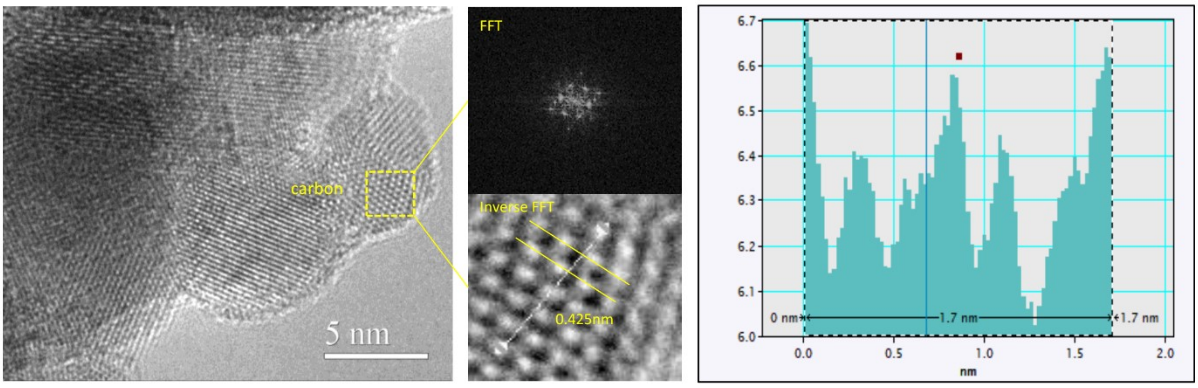

Fig. S6. HRTEM image of Pd/SnO_2@C presenting crystalline carbon site.

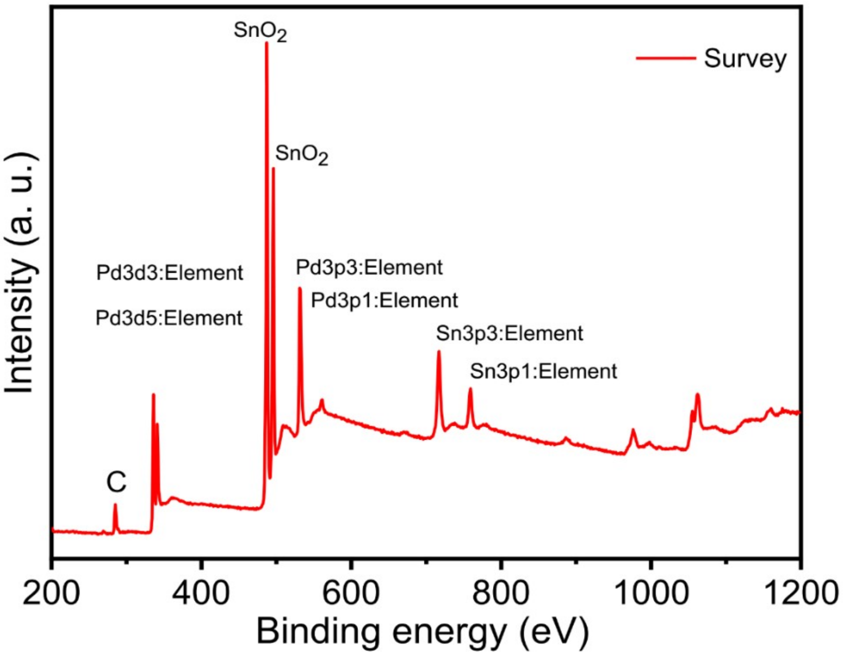

Fig. S7. XPS Survey spectrum of Pd/SnO_2@C.

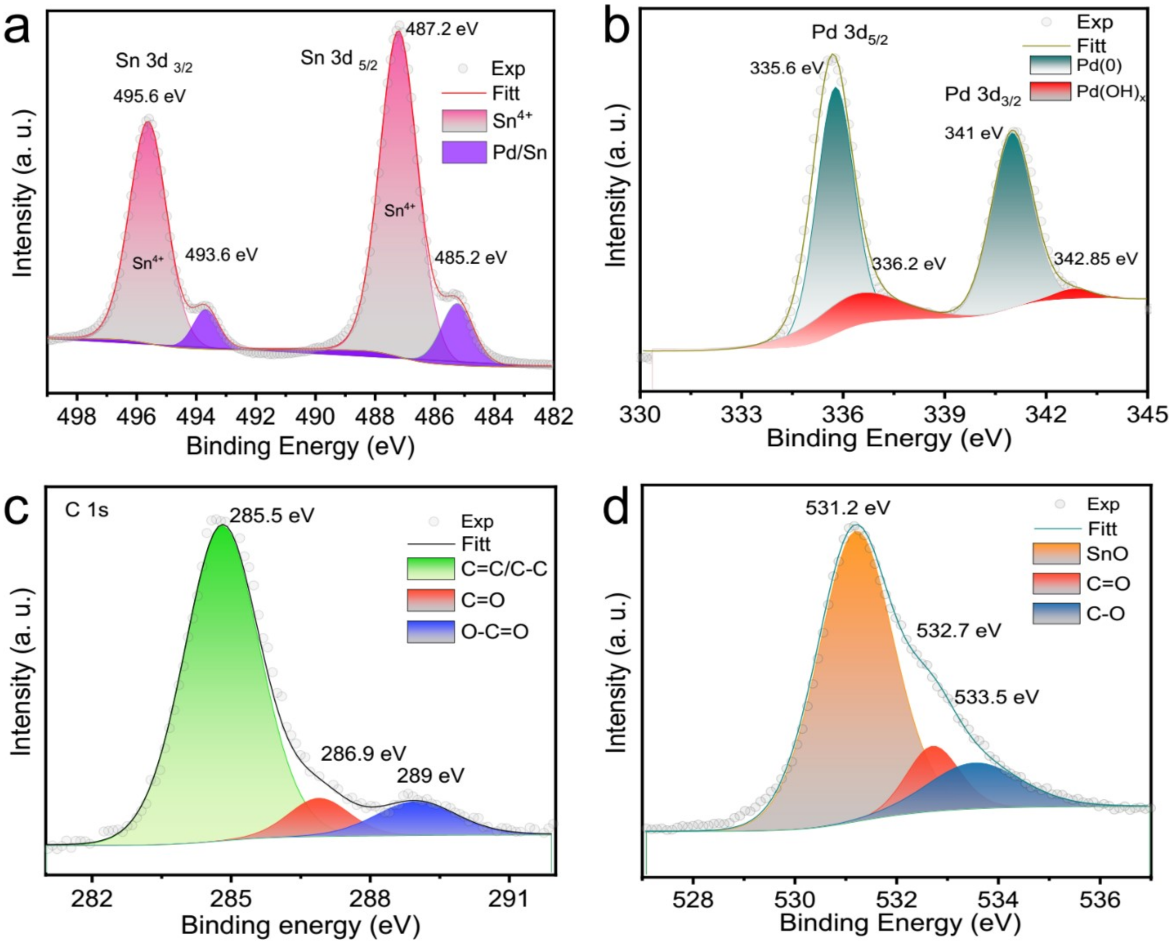

Fig. S8. HR XPS spectrums of Sn 3d (a), Pd 3d (b), C 1s (c) and O 1s (d) for Pd/SnO_2@C.

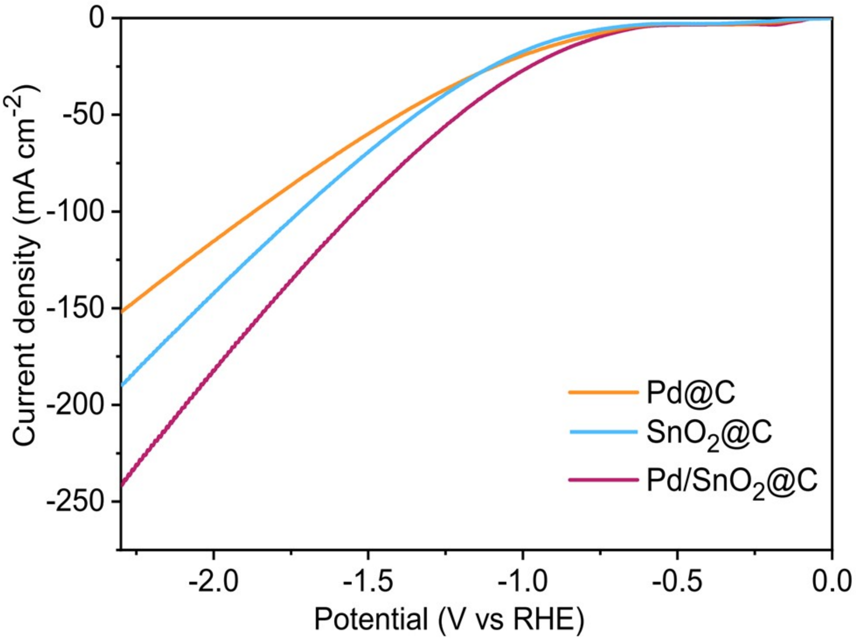

Fig. S9. LSV curves for all as-synthesized catalysts under CO_2 supply.

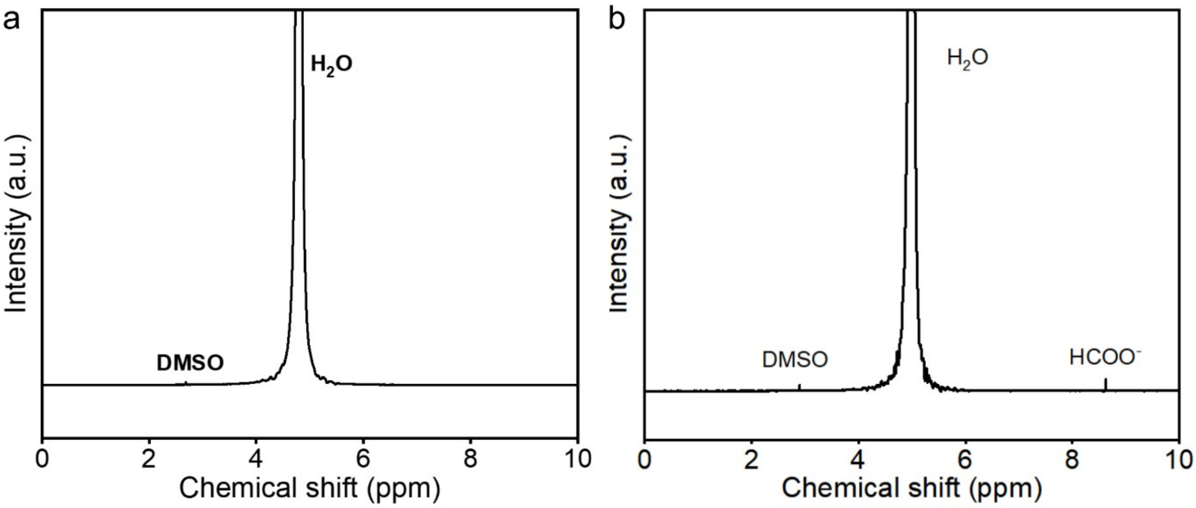

Fig. S10. NMR spectra under the supply of Ar (a) and after the supply of CO_2.

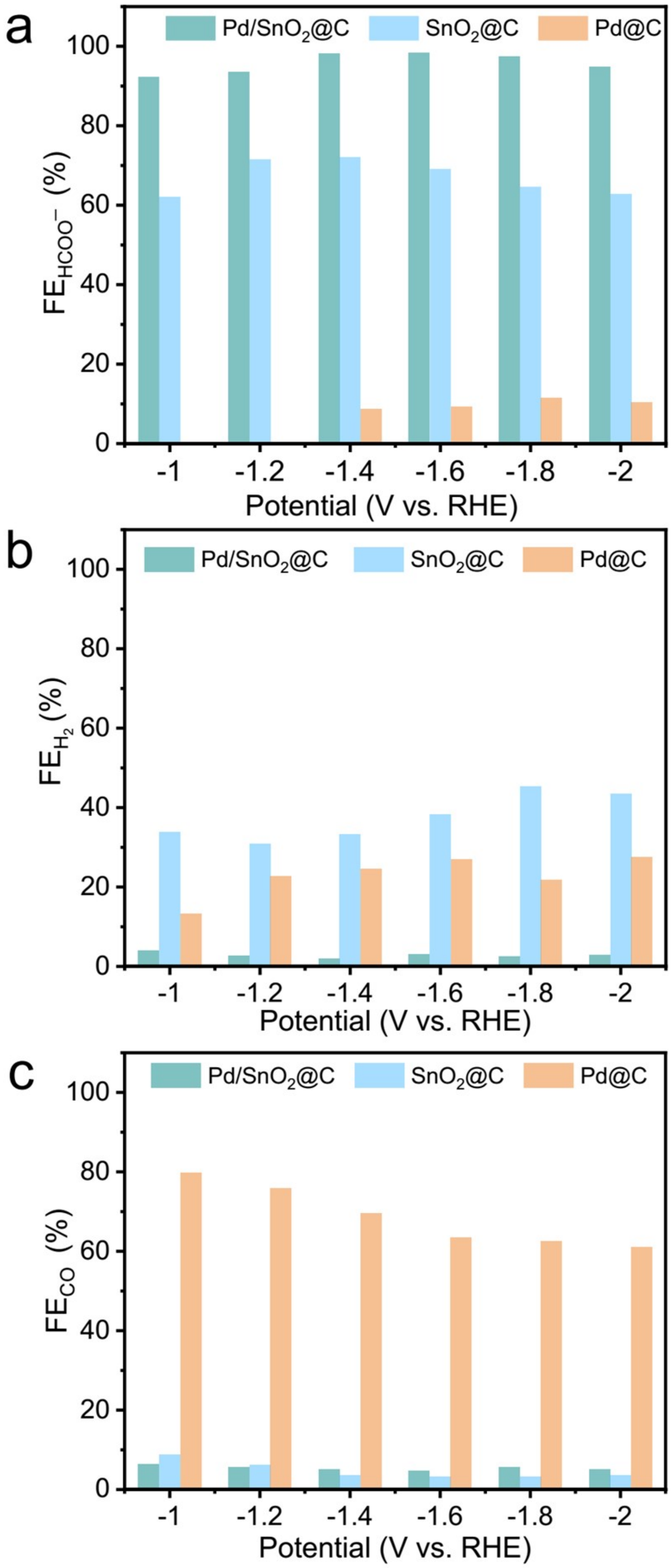

Fig. S11. Comparison of eCO_2RR Faradaic Efficiencies (FEs) for all three prepared catalytic materials: FEs for Formate ($HCOO^-$) (a), FEs for hydrogen (H_2) (b), and FEs for carbon monoxide (CO) (c).

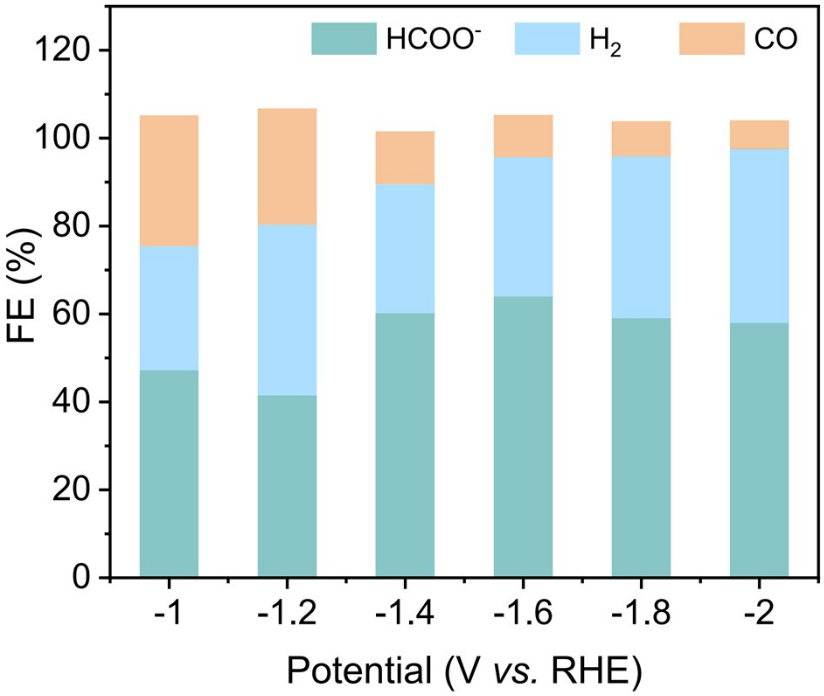

Fig. S12. FE's of different products based on H-type cell eCO_2RR.

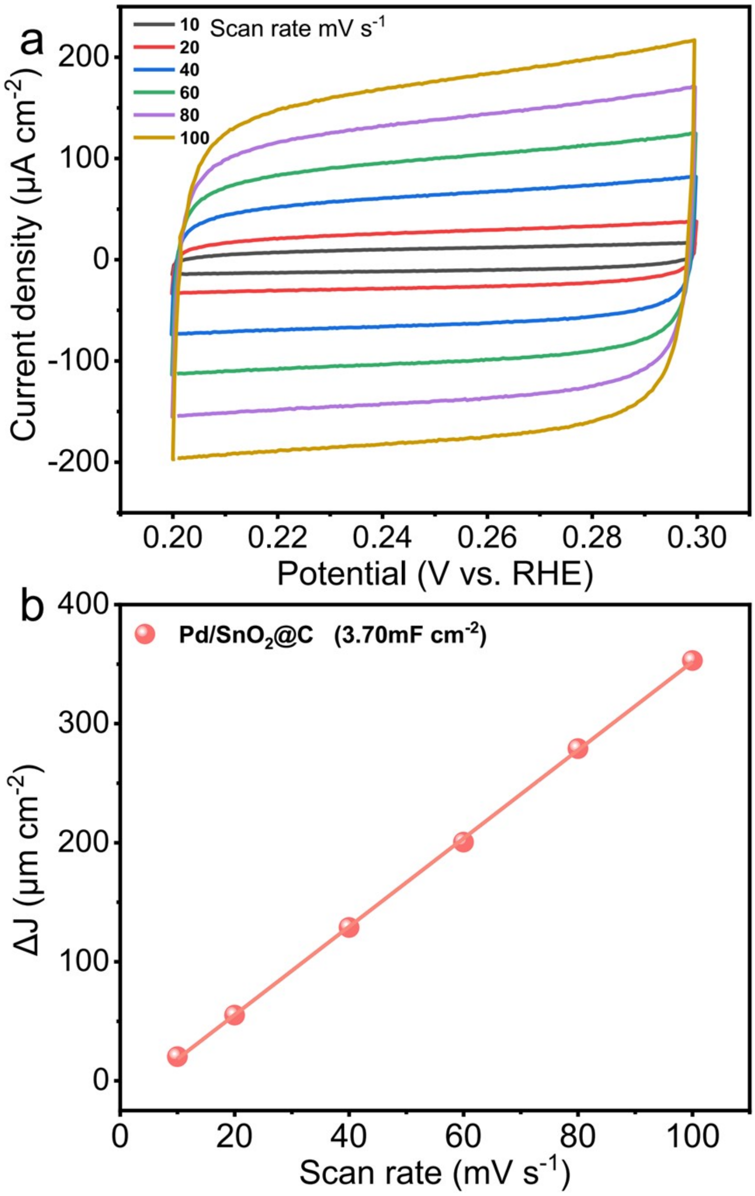

Fig. S13. Double layer capacitance investigation of Pd/SnO_2@C. Cyclic voltammetry curves at different scan rates (a). Overall response of current density against different scan rates (b).

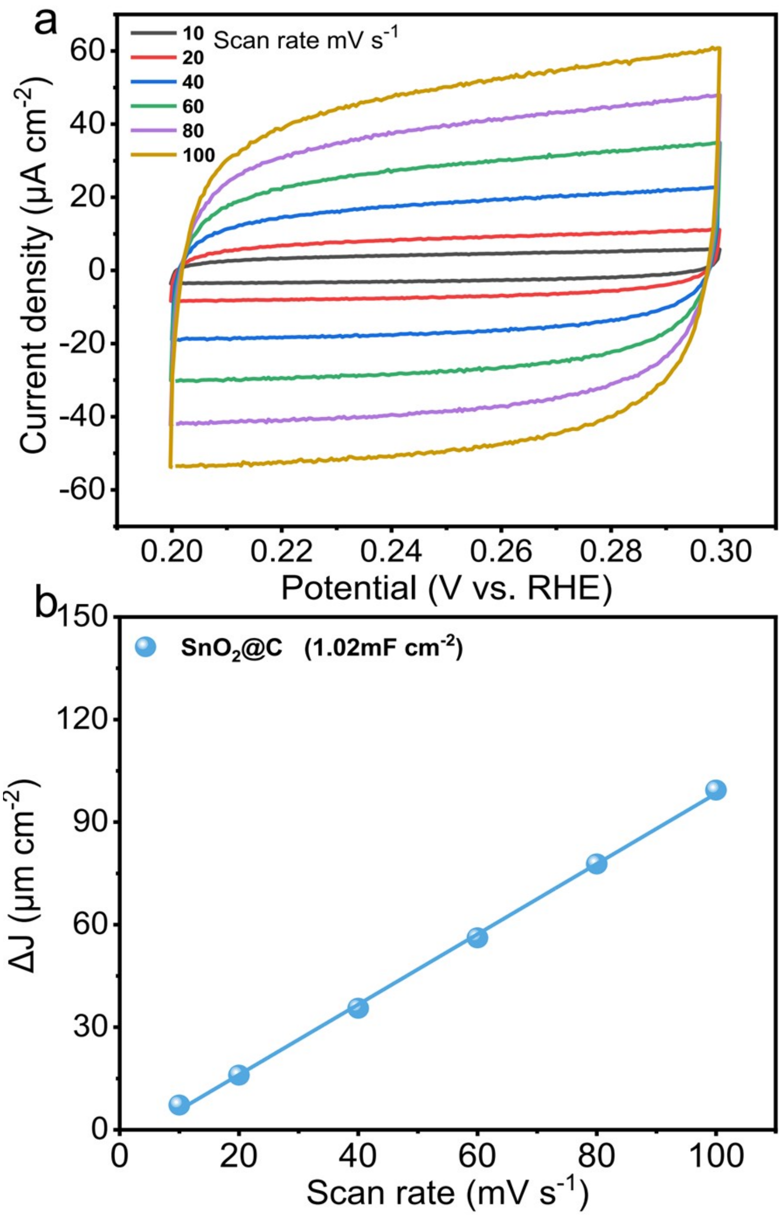

Fig. S14. Double layer capacitance investigation of SnO_2@C. Cyclic voltammetry curves at different scan rates (a). Overall response of current density against different scan rates (b).

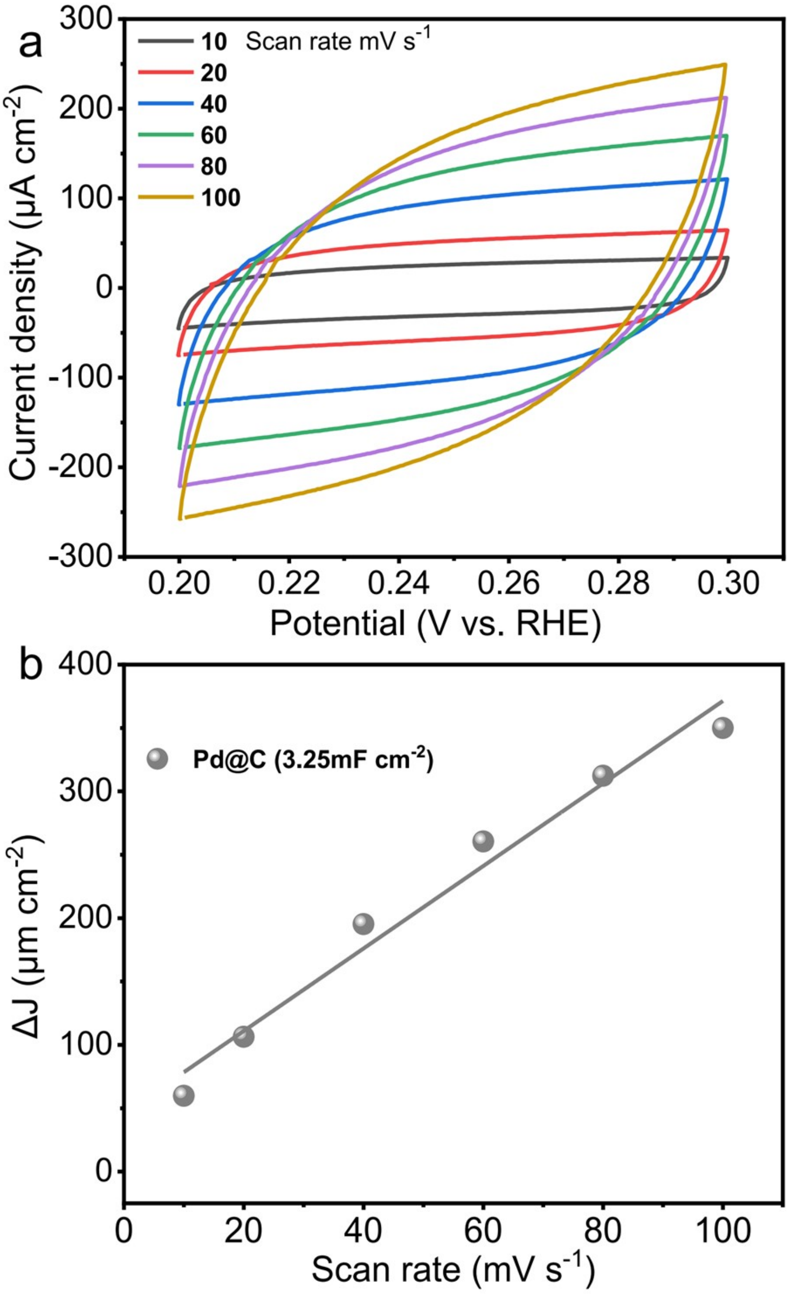

Fig. S15. Double layer capacitance investigation of Pd@C. Cyclic voltammetry curves at different scan rates (a). Overall response of current density against different scan rates (b).

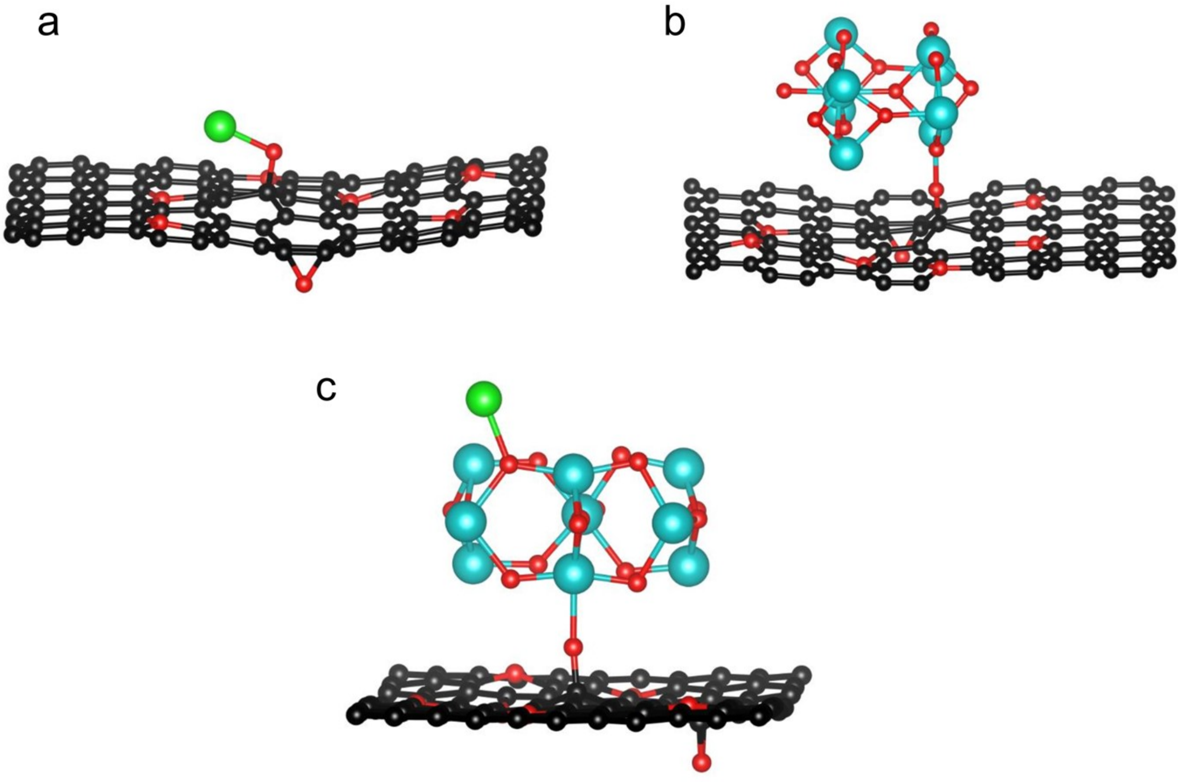

Fig. S16. Models structures of Pd@C (a), SnO_2@C (b) and Pd/SnO_2@C (c).

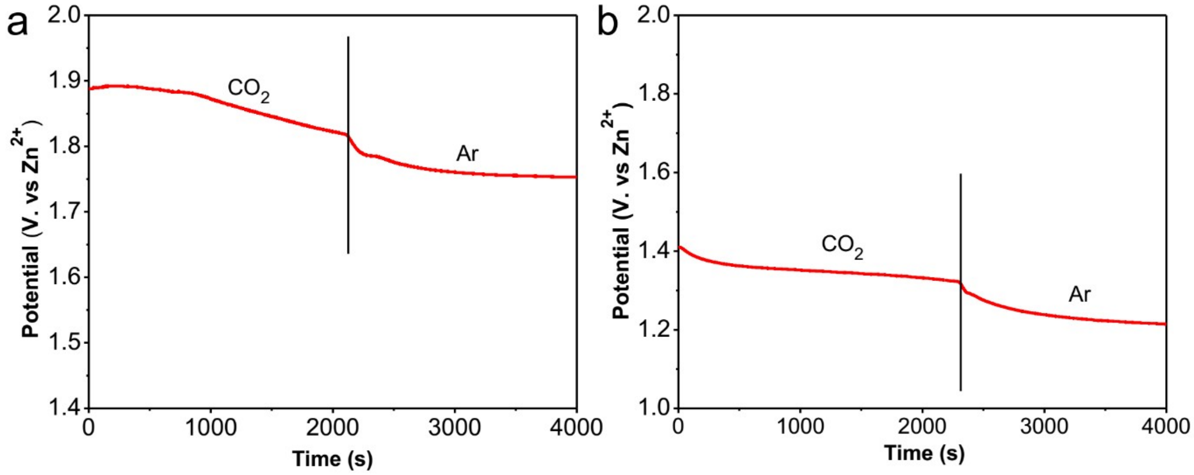

Fig. S17. OCP curves presenting response against CO_2 and Ar supply for Pd@C (a) and SnO_2@C (b) based on homemade flow type cell.

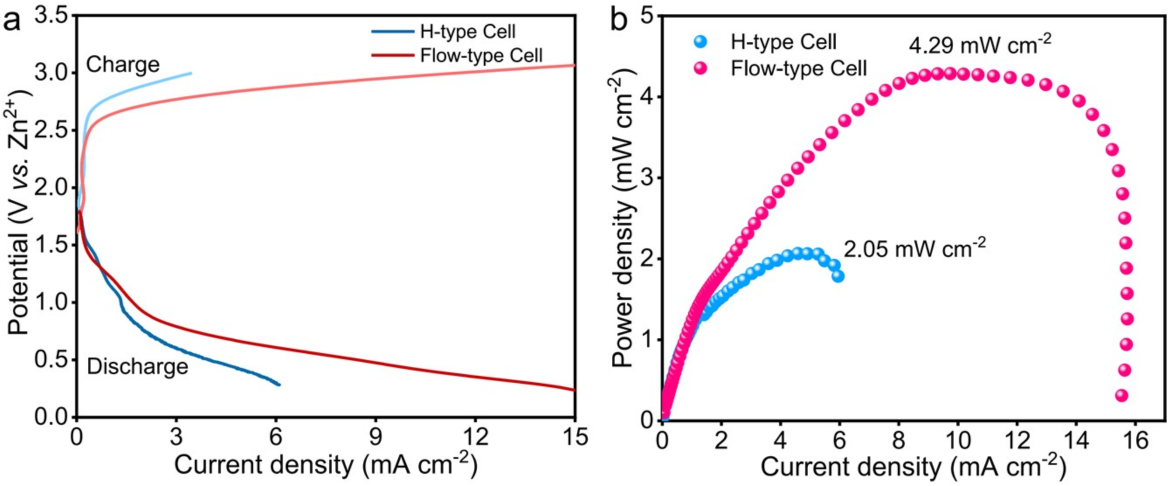

Fig. S18. Polarization charge-discharge curves for both H-cell and flow cell based on aqueous Zn-CO_2 batteries (a) and corresponding power densities curves (b).

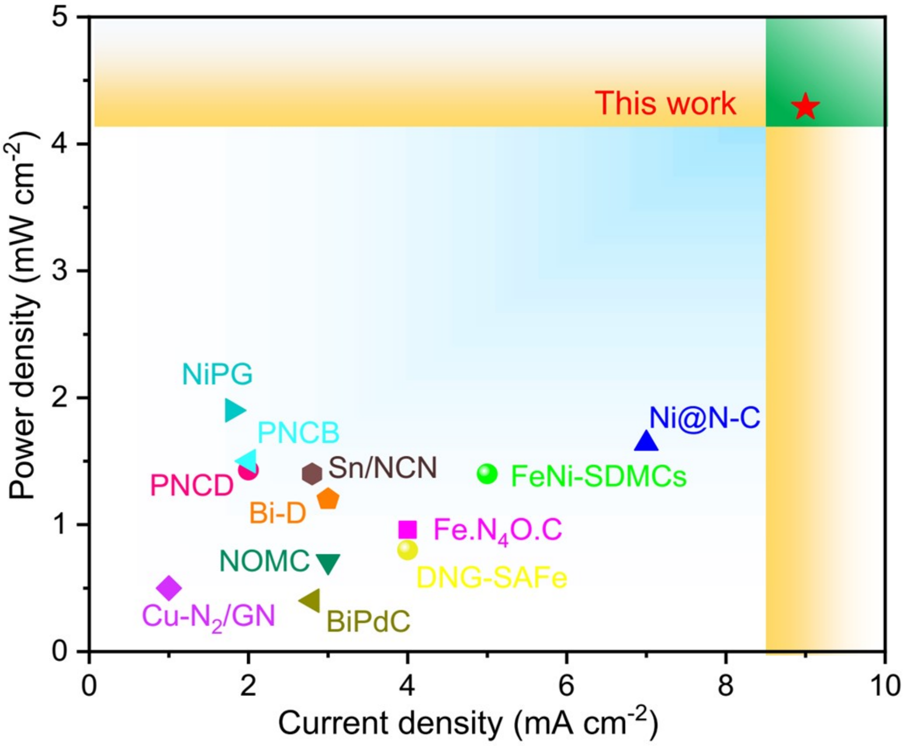

Fig. S19. Comparison of power densities with previously reported works

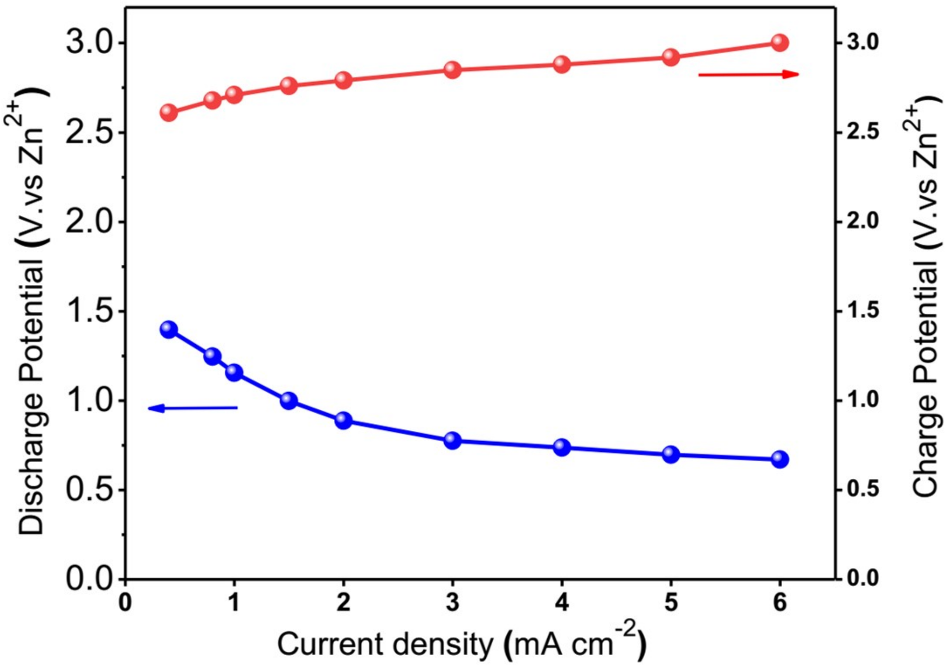

Fig. S20. Overall charge-discharge response at different current rate based on flow type cell.

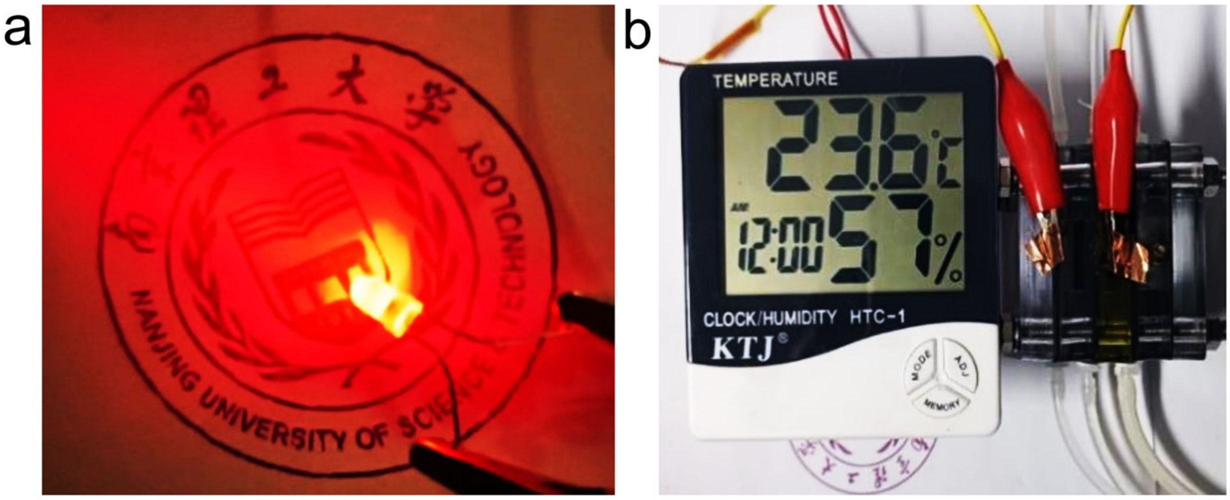

Fig. 21S. Digital photograph of a single bulb illuminated by a 3-series of aqueous Zn-CO_2 batteries (a) and a digital clock power by single aqueous Zn-CO_2 battery (b).

Figure S22. pH values measured at different pre-saturating CO_2 time.

Table S1. Energy efficiencies (EE) of the aqueous rechargeable reversible Zn-CO_2 battery at different applied current densities.

Current (mA)	Discharge Voltage (V)	FE of $HCOO^-$ （%）	FE of CO （%）	FE of H_2 （%）	Charge Voltage (V)	EE (%)	EE‘ (%)	EE“ (%)
1	1.16	62.84	20.85	25.1	2.73	73.06	83.38	95.64
2	0.91	86.13	13.01	6.05	2.79	73.67	80.01	82.90
3	0.82	89.44	15.86	4.04	2.83	71.01	78.60	80.51
4	0.766	95.86	9.42	3.159	2.87	71.12	75.61	77.08
5	0.729	93.69	9.98	2.93	2.92	67.65	72.31	73.66
6	0.679	92.22	9.04	2.59	3	63.53	67.65	68.80

Note: EE is calculated based on $HCOO^-$, splitting in the cell; EE‘ is calculated when CO are also accounted with $HCOO^-$ and EE‘‘ is calculated when water splitting also accounted with $HCOO^-$ and CO

Table S2. Comparison of aqueous reversible Zn-CO$_2$ battery performance with previously reported works.

Catalyst	**Catholyte**	**Anolyte**	**Product**	**FE (%)**	**Power density (mW cm^{-2})**	**Energy efficiency (%)**	**Energy density (Wh kg^{-1})**	**Ref.**
Pd/SnO$_2$@C-MOF	**0.8M KHCO$_3$**	**6M KOH + 0.2M Zn(Ac)$_2$**	**Formate**	**95.4**	**4.29**	**95.64**	**827.3**	**This work**
3D porous Pd	1M NaCl + 0.1M NaAc	1M KOH + 0.02M Zn(Ac)$_2$	Formate	81.2	N/A	81.2	788	6
CoPc@DNHCS-8	0.8M KHCO$_3$	0.8M KOH + 0.02M Zn(Ac)$_2$	CO	95.68	1.02	46.7	583	7
Ir@Au	0.8M KHCO$_3$	0.8M KOH + 0.02M Zn(Ac)$_2$	CO	90	N/A	68	583	8
NiFe DASC	2M KCl	2M KOH + 0.02M Zn(Ac)$_2$	CO	90.6	1.35	56.3	N/A	9
Cu$_3$P/C	0.1M KHCO$_3$	4M NaOH	CO	47	2.26	N/A	N/A	10
CB-NGC-2	0.8M KHCO$_3$ + 0.2MZn(Ac)$_2$	0.8M KOH + 0.2M Zn(Ac)$_2$	CO	91	0.51	N/A	N/A	11
CNTs@Cu	[EMIM][BF$_4$]	EMIM][BF$_4$]	CH$_4$	93.3	1.89	N/A	208.7	12
CHF	[EMIM][BF$_4$]	[EMIM][BF$_4$]	CH$_4$	94	0.8	N/A	288.3	13
Ni–Nx-2D/NPC	1M KHCO$_3$	1M KOH + 0.02M Zn(Ac)$_2$	CO	~100	N/A	53.7	N/A	14
ZrO2@Ni-NC	0.5M KHCO$_3$	6M KOH + 0.02M Zn(Ac)$_2$	CO	98.6	N/A	76.4	594	15
Bi-D	2M KHCO$_3$ + 0.02M Zn(Ac)$_2$	2M KOH + 0.02M Zn(Ac)$_2$	Formate	93.9	1.16	N/A	N/A	16
s-SnLi	6M KOH + 0.02M Zn(Ac)$_2$	6M KOH + 0.02M Zn(Ac)$_2$	Formate	92	1.24	N/A	158	17
VO-rich N–SnO$_2$ NS	0.1M KHCO$_3$	N/A	Formate	83	3.67	56	~550	18

CA/N–Ni	0.5M $KHCO_3$	6M KOH + 0.2M $Zn(Ac)_2$	CO	98	0.5	57	N/A	19
Zn/NC NS	0.5M $KHCO_3$	6M KOH + 0.2M $Zn(Ac)_2$	CO	95	1.8	59	622	20
Ni–N_3-NCNFs	0.5M $KHCO_3$	6M KOH + 0.2M $Zn(Ac)_2$	CO	96.6	1.05	N/A	N/A	21
NOMC	0.8M $KHCO_3$	6M KOH + 0.2 M $Zn(Ac)_2$	CO	~100	0.71	52.8	583	22
NiPG	3M $KHCO_3$ + 1.5M KCl	6M KOH + 0.2M $Zn(Ac)_2$	CO	66	0.28	61	523	23
PNCB	2M $KHCO_3$ + 0.02M $Zn(Ac)_2$	2M KOH + 0.02M $Zn(Ac)_2$	Formate	94.8	1.43	45	N/A	24
In/ZnO@C	0.8M $KHCO_3$	0.8M KOH + 0.02M $Zn(Ac)_2$	Formate	90	1.32	61.8	495	25
Cu–N_2/GN	0.1M $KHCO_3$	6M KOH + 0.2M $Zn(Ac)_2$	CO	81	0.6	61	624	26
Ni_9Cu_1@NCNTs/CFM	0.25M $KHCO_3$	N/A	CO	97	0.65	N/A	N/A	27
Fe-SA/BNC	0.8M $KHCO_3$	0.8M KOH + 0.02 M $Zn(Ac)_2$	CO	94	1.18	63.6	583	28
Fe–P–C	1M $KHCO_3$	6M KOH + 0.02M $Zn(Ac)_2$	CO	95	0.85	75	231.8	29
Fe_1NC/S_1-1000	0.8M $KHCO_3$	0.8M KOH + 0.02M $Zn(Ac)_2$	CO	96	0.526	N/A	N/A	30
HPC-Co/CoPc	1M $KHCO_3$	6M KOH + 0.2M $Zn(Ac)_2$	CO+H_2	N/A	2.67	67.5	533	31
Fe–Ni–N–C	0.8M $KHCO_3$	0.8MKOH + 0.02M $Zn(Ac)_2$	CO	93.4	N/A	65	583	32

References

1. G. Kresse and J. Hafner, *Physical Review B*, 1993, **48**, 13115-13118.
2. G. Kresse and J. Furthmüller, *Physical Review B*, 1996, **54**, 11169-11186.
3. G. Kresse and D. Joubert, *Physical Review B*, 1999, **59**, 1758-1775.
4. J. P. Perdew, K. Burke and M. Ernzerhof, *Phys. Rev. Lett.*, 1996, **77**, 3865-3868.
5. K. S. Exner, J. Anton, T. Jacob and H. Over, *Electrochimica Acta*, 2014, **120**, 460-466.
6. J. Xie, X. Wang, J. Lv, Y. Huang, M. Wu, Y. Wang and J. Yao, *Angew. Chem. Int. Ed.*, 2018, **57**, 16996-17001.
7. S. Gong, W. Wang, C. Zhang, M. Zhu, R. Lu, J. Ye, H. Yang, C. Wu, J. Liu, D. Rao, S. Shao and X. Lv, *Adv. Funct. Mater.*, 2022, **32**, 2110649.
8. X. Wang, J. Xie, M. A. Ghausi, J. Lv, Y. Huang, M. Wu, Y. Wang and J. Yao, *Adv. Mater.*, 2019, **31**, 1807807.
9. Z. Zeng, L. Y. Gan, H. Bin Yang, X. Su, J. Gao, W. Liu, H. Matsumoto, J. Gong, J. Zhang, W. Cai, Z. Zhang, Y. Yan, B. Liu and P. Chen, *Nat. Commun.*, 2021, **12**, 4088.
10. M. Y. Peng, S. Q. Ci, P. Shao, P. W. Cai and Z. H. Wen, *J. nanosci. nanotechnol.*, 2019, **19**, 3232-3236.
11. X. Hao, X. An, A. M. Patil, P. Wang, X. Ma, X. Du, X. Hao, A. Abudula and G. Guan, *ACS Appl. Mater. Interfaces*, 2021, **13**, 3738-3747.
12. Y. Chen, Y. Mei, M. Li, C. Dang, L. Huang, W. Wu, Y. Wu, X. Yu, K. Wang, L. Gu, L. Liu and X. Cao, *Green Chem.*, 2021, **23**, 8138-8146.
13. K. Wang, Y. Wu, X. Cao, L. Gu and J. Hu, *Adv. Funct. Mater.*, 2020, **30**, 1908965.
14. Z. Zeng, A. G. A. Mohamed, X. Zhang and Y. Wang, *Energy Technology*, 2021, **9**, 2100205.
15. X. Wang, S. Feng, W. Lu, Y. Zhao, S. Zheng, W. Zheng, X. Sang, L. Zheng, Y. Xie, Z. Li, B. Yang, L. Lei, S. Wang and Y. Hou, *Adv. Funct. Mater.*, 2021, **31**, 2104243.
16. Y. Wang, Z. Huang, Y. Lei, J. Wu, Y. Bai, X. Zhao, M. Liu, L. Zhan, S. Tang, X. Zhang, F. Luo and X. Xiong, *Chem. Commun.*, 2022, **58**, 3621-3624.
17. S. Yan, C. Peng, C. Yang, Y. Chen, J. Zhang, A. Guan, X. Lv, H. Wang, Z. Wang, T.-K. Sham, Q. Han and G. Zheng, *Angew. Chem. Int. Ed.*, 2021, **60**, 25741-25745.
18. Z. Li, A. Cao, Q. Zheng, Y. Fu, T. Wang, K. T. Arul, J.-L. Chen, B. Yang, N. M. Adli, L. Lei, C.-L. Dong, J. Xiao, G. Wu and Y. Hou, *Adv. Mater.*, 2021, **33**, 2005113.
19. Y. Zhang, X. Wang, S. Zheng, B. Yang, Z. Li, J. Lu, Q. Zhang, N. M. Adli, L. Lei, G. Wu and Y. Hou, *Adv. Funct. Mater.*, 2021, **31**, 2104377.

20. J. Chen, Z. Li, X. Wang, X. Sang, S. Zheng, S. Liu, B. Yang, Q. Zhang, L. Lei, L. Dai and Y. Hou, *Angew. Chem. Int. Ed.*, 2022, **61**, e202111683.
21. W. Zheng, Y. Wang, L. Shuai, X. Wang, F. He, C. Lei, Z. Li, B. Yang, L. Lei, C. Yuan, M. Qiu, Y. Hou and X. Feng, *Adv. Funct. Mater.*, 2021, **31**, 2008146.
22. S. Gao, Y. Liu, Z. Xie, Y. Qiu, L. Zhuo, Y. Qin, J. Ren, S. Zhang, G. Hu, J. Luo and X. Liu, *Small Methods*, 2021, **5**, 2001039.
23. R. Yang, J. Xie, Q. Liu, Y. Huang, J. Lv, M. A. Ghausi, X. Wang, Z. Peng, M. Wu and Y. Wang, *J. Mater. Chem. A*, 2019, **7**, 2575-2580.
24. Y. Wang, L. Xu, L. Zhan, P. Yang, S. Tang, M. Liu, X. Zhao, Y. Xiong, Z. Chen and Y. Lei, *Nano Energy*, 2022, **92**, 106780.
25. X. Teng, Y. Niu, S. Gong, M. Xu, X. Liu, L. Ji and Z. Chen, *Materials Chemistry Frontiers*, 2021, **5**, 6618-6627.
26. W. Zheng, J. Yang, H. Chen, Y. Hou, Q. Wang, M. Gu, F. He, Y. Xia, Z. Xia, Z. Li, B. Yang, L. Lei, C. Yuan, Q. He, M. Qiu and X. Feng, *Adv. Funct. Mater.*, 2020, **30**, 1907658.
27. S. Shen, C. Han, B. Wang and Y. Wang, *Chin. Chem. Lett.*, 2022, **33**, 3721-3725.
28. S. Liu, M. Jin, J. Sun, Y. Qin, S. Gao, Y. Chen, S. Zhang, J. Luo and X. Liu, *Chem. Eng. J.*, 2022, **437**, 135294.
29. S. Liu, L. Wang, H. Yang, S. Gao, Y. Liu, S. Zhang, Y. Chen, X. Liu and J. Luo, *Small*, 2022, **18**, 2104965.
30. T. Wang, X. Sang, W. Zheng, B. Yang, S. Yao, C. Lei, Z. Li, Q. He, J. Lu and L. Lei, *Adv. Mater.*, 2020, **32**, 2002430.
31. W. Ni, Z. Liu, X. Guo, Y. Zhang, C. Ma, Y. Deng and S. Zhang, *Appl. Catal. B: Environ.*, 2021, **291**, 120092.
32. L. Jiao, J. Zhu, Y. Zhang, W. Yang, S. Zhou, A. Li, C. Xie, X. Zheng, W. Zhou, S.-H. Yu and H.-L. Jiang, *J. Am. Chem. Soc.*, 2021, **143**, 19417-19424.